Emergent optical plasmons at the surface of a doped three-dimensional topological insulator

Tong Wei [1,*] Yujie Liu [1,*] Ping Cui [1] Xiaoguang Li [2,†] and Zhenyu Zhang [1,‡]

[1]*International Center for Quantum Design of Functional Materials (ICQD), Hefei National Research Center for Physical Sciences at the Microscale and CAS Center for Excellence in Quantum Information and Quantum Physics, University of Science and Technology of China, Hefei, Anhui 230026, China*

[2]*Institute for Advanced Study, Shenzhen University, Shenzhen 518060, China*

(Received 5 November 2021; revised 22 April 2022; accepted 22 April 2022; published 5 May 2022)

The conduction electrons in the topologically nontrivial surface states of three-dimensional topological insulators have been actively exploited to exhibit emergent exotic properties and functionalities. The existence of a trivial two-dimensional electron gas near the surface has also been widely established, stemming from surface carrier doping of the topological insulators. Here we investigate theoretically the coupling between the electrons in the topological surface states and two-dimensional electron gas, and reveal that the helical nature of the former can be effectively shared with the latter through proximity effect. Next we examine the collective modes of the combined system and predict an optical plasmon mode rooted in the enhanced interband transitions of the nontrivial bands with the same helicity. The emergence of the interband transitions also introduce pronounced variations in the Dirac plasmon mode of the topological surface states, characterized by its gapped feature. These findings may find important applications in plasmonic and spintronic devices.

DOI: 10.1103/PhysRevB.105.205408

I. INTRODUCTION

Three-dimensional topological insulators possessing topological surface states (TSSs) with spin-momentum locking have been well-established in recent studies [1–6]. Various exotic aspects of the plasmonic excitations associated with the TSSs have also been actively investigated. Compelling examples include the predictions of a hybrid spin-plasmon [7] and an optical plasmon mode [8], and experimental observations of the Dirac plasmon [9–11] and anomalous acoustic plasmon modes [12], all at the surface or a thin film of topological insulators. A very recent experimental study has also reported the observation of multiple plasmon modes in topological nodal-line semimetals [13]. These developments have substantially enriched our knowledge of plasmonics in quantum topological matters.

Beyond the TSSs, another widespread feature associated with a three-dimensional topological insulator is the existence of a two-dimensional electron gas (2DEG) near the surface, originating from the unavoidable electron doping of both the surface and the bulk [3,5,14]. The physical origin of such an electron gas accumulation was identified much earlier, commonly present at the charged surface, as manifested by band bending near the surface [15–17]. When specified to the three-dimensional topological insulators, the 2DEG also exhibits Rashba-type spin splitting in its electronic states [18–22]. Given their close spatial vicinity, it is natural and conceptually intriguing to explore the coupling between the TSSs and trivial states in the electron gas, both in the ground state and plasmonic excitations.

In this paper, we present a comprehensive theoretical study of the coupling between the TSSs and 2DEG, with intriguing and inherently connected findings. We first reveal that, as a fingerprint of the nontrivial topology, the helicity of the former is propagated into the latter through effective proximity effect. Next we predict that the combined system harbors an optical plasmon mode, which is attributed to the interband transitions between the two types of surface states having the same helicity, with dominant contributions from the inverted region of the hybrid bands. We further show that the existence of the interband transitions necessarily introduces pronounced variations in the more commonly studied Dirac plasmon mode associated with the TSSs, characterized by its gapped feature. The existence and tunability of the plasmon modes can be experimentally exploited and may find important applications in plasmonic and spintronic devices based on topological insulators.

II. HYBRIDIZATION BETWEEN TOPOLOGICAL SURFACE STATE AND TWO-DIMENSIONAL ELECTRON GAS

An illustration of the system is shown in Fig. 1(a), with the 2DEG and the TSSs of the topological insulator shown in Figs. 1(b)–1(d), respectively. We first introduce the following effective Hamiltonian to describe the TSS with a k-dependent mass [2,8,23,24]:

$$H_{\mathrm{TSS}} = Ak^2\sigma_z + v_F(\boldsymbol{\sigma}\times\boldsymbol{k})\cdot\hat{\boldsymbol{z}} = \begin{pmatrix} Ak^2 & iv_Fk_- \\ -iv_Fk_+ & -Ak^2 \end{pmatrix}, \quad (1)$$

*These authors contributed equally to this work.
†Corresponding author: xgli@szu.edu.cn
‡Corresponding author: zhangzy@ustc.edu.cn

 ©2022 American Physical Society

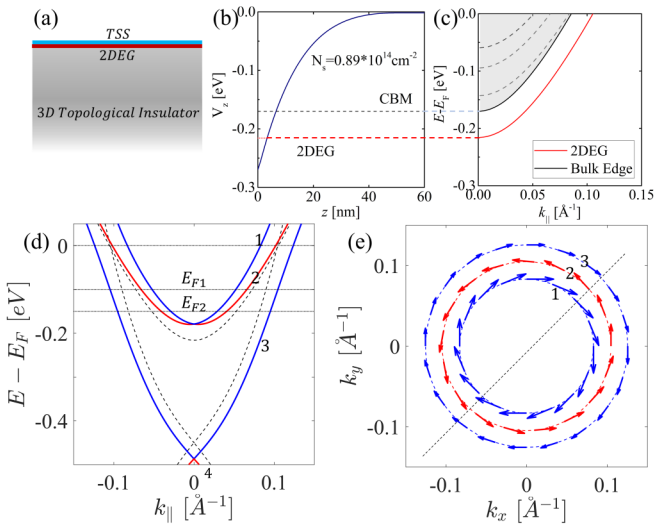

FIG. 1. (a) Schematic of the coexisting TSS and 2DEG at the surface of a heavily electron-doped 3D topological insulator. (b) One-electron potential V_z in the accumulation layer at the given surface density specified. (c) Calculated dispersions of the spin-degenerate 2DEG states (dashed and red lines). (d) The decoupled (dashed) and coupled (solid) dispersions of the TSS and 2DEG states. (e) In-plane spin texture of the coupled bands cross the Fermi surface as shown in (d).

where A is the mass term, v_F is the effective velocity, $\hat{z}$ is the unit vector along the normal direction of the 2D plane, $\boldsymbol{\sigma}$ is the Pauli matrix, and $k_\pm = k_x \pm ik_y$ are the 2D wave vectors. In Fig. 1(d), the massive Dirac cone marked by the dashed black lines is the TSS from Eq. (1) by setting $A = 35$ eV $\times$ Å^2 and $v_F = 2.3$ eV $\times$ Å, which fits well the experimentally observed TSS of Bi_2Se_3 in the absence of the 2DEG (see Fig. S2 in the Supplemental Material (SM) [25]). The system Bi_2Se_3 is used as a prototypical example in the present paper, and the Dirac point is below the Fermi level due to the electron doping of the system [14].

Next, the 2DEG states are obtained self-consistently by solving the combined Poisson's and Schrödinger equations [16,17], a widely established approach invoked recently in studying surface electronic properties of the topological insulator [14] (see more details in the SM [25]). In Fig. 1(b), we show the effective one-electron potential V_z that confines the conduction band states into a number of discrete levels, and the corresponding spin-degenerate 2DEG states are illustrated in Fig. 1(c). By specifying the surface charge density at $N_s = 0.89 \times 10^{14}$cm^{-2} [25], we have only one state (the red line) below the conduction band minimum (CBM) associated with electron doping of the bulk. The other 2DEG states (grey dashed line) with higher energies above the CBM will penetrate deeper into the bulk [16,17] and will be readily screened by or hybrid with the carriers in the bulk. Therefore, we will concentrate on the lowest 2DEG state that, in principle, can dominantly couple with the TSS. Considerations of more 2DEG states will be presented later.

So far, the TSS and 2DEG states are introduced independently without coupling, as indicted by the black dashed lines in Fig. 1(d). When their coupling is switched on, we have the following interacting Hamiltonian:

$$H_{\text{eff}} = \begin{pmatrix} H_{TSS} - \mu_{\text{TSS}} & V_1\sigma_0 \\ V_1^*\sigma_0 & H_{\text{2DEG}} \end{pmatrix}, \tag{2}$$

where μ_{TSS} is the chemical potential of the TSS, V_1 is the coupling strength between the TSS and 2DEG state, σ_0 is the 2×2 identity matrix, and H_{2DEG} represents the lowest-lying 2DEG state in Fig. 1(c). In Fig. 1(d), the solid lines are the coupled states from Eq. (2) and several intriguing features can be observed as follows. Here we have chosen $V_1 = 100$ meV, which yields band splittings comparable to the experimental observations [18–22], and μ_{TSS} is set to be 450 meV.

First, the spin-degenerate 2DEG state now exhibits the Rashba-type splitting due to its coupling with the TSS, as experimentally observed at the surfaces of inherently or intentionally doped 3D topological insulators [18–22]. The detailed in-plane spin textures for the three bands 1–3 crossing the Fermi level are further displayed in Fig. 1(e). Intriguingly, the robust helical nature of the TSS (band 3) persists and further propagates into the spin-split 2DEG states (bands 1 and 2) through effective proximity coupling, qualitatively explaining existing experimental observations [18,21]. Furthermore, beyond the in-plane spin textures, the behavior of the out-plane spin component (σ_z) in the TSS is also shared by the 2DEG states. In Figs. S3 of the SM, we show the three projected spin components of the electrons in bands 1–3 of Fig. 1(d), along the black dashed line in Fig. 1(e). In all three bands, only those states near $k = 0$ (namely, the Dirac point) have pure in-plane spin components ($\sigma_\parallel = 1$), and the σ_z components gradually develop as the momentum increases, again qualitatively consistent with existing experiments [4,21]. We further analytically derive that $\sigma_\parallel = \sigma_z$ at $k = v_F/A$, which coincides with the numerical results in Figs. S3.

Second, the hybrid bands now open a gap at the crossing points, accompanied by a band inversion between the TSS and 2DEG state [bands 1 and 3 in Fig. 1(d)]. Importantly, such a band inversion can substantially enhance the overlapping integral of the interband transitions and facilitate the creation of the electron-hole (e-h) pairs accordingly. As a consequence, the system can harbor the formation of plasmon modes associated with the e-h pairs, particularly when the e-h pairs interact coherently [8,26]. It is also worth pointing out that the band inversion only takes place between bands 1 and 3 with the same helicity (helicity selection rule), as shown in Fig. 1(d), a point to be further justified from the overlapping integrals in Fig. 3(b). Therefore, owing to their degenerate helicity, the interband plasmon excitations are always accompanied by a transverse spin mode known as a hybrid spin-plasmon mode [7]. We note that such hybrid spin-plasmon modes could also emerge at the surfaces or interfaces with strong Rashba spin-orbital coupling induced by spatial inversion symmetry breaking [27,28]. Furthermore, it should be very intriguing to investigate whether the spin-plasmon mode also possesses definitive helicity, an objective to be explored in future studies.

When the Fermi level is far away from the Dirac point, the nonlinear term in the effective model for the surface state becomes significant, as represented by the warping effect [29]. In this case, the Hamiltonian describing the TSS can be generalized to $H(\boldsymbol{k}) = E_0(\boldsymbol{k}) + v_{\boldsymbol{k}}(k_x\sigma_y - k_y\sigma_x) + \lambda/2(k_+^3 + k_-^3)$.

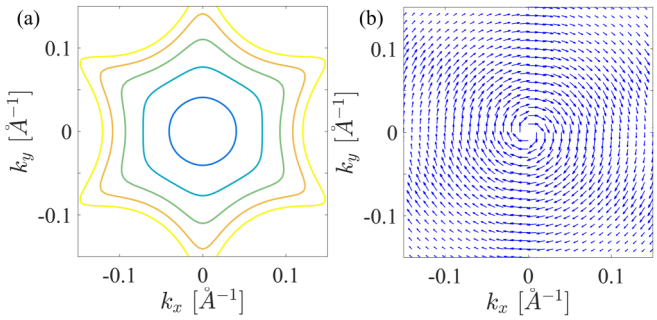

FIG. 2. (a) Energy contours of the topological surface state with the inclusion of the warping effect. (b) The corresponding in-plane spin texture of the topological surface state, with the arrow length representing the relative magnitude of the spin. Here, the electron effective mass m^* is given by the bare electron mass, $\alpha = 0$, and $\lambda = 100\,\text{eV} \times \text{Å}^3$.

The corresponding constant energy contours of the TSS and its in-plane spin texture are given in Fig. 2, using typical system parameters as given in the caption. Here we note that, first, inclusion of the warping effect still preserves the in-plane spin-momentum locking nature of the TSS, even though it alters the magnitudes of the in-plane spin component along the warping direction. Second, the helicity selection rule is rooted in the band inversion between the 2DEG and TSS. With the inclusion of the warping effect, the dispersion of the TSS becomes steeper but the band inversion is still present. Therefore, the warping effect will not compromise the helicity selection rule either. Finally, the plasmon dispersion is expected to become anisotropic in systems with strong warping effects.

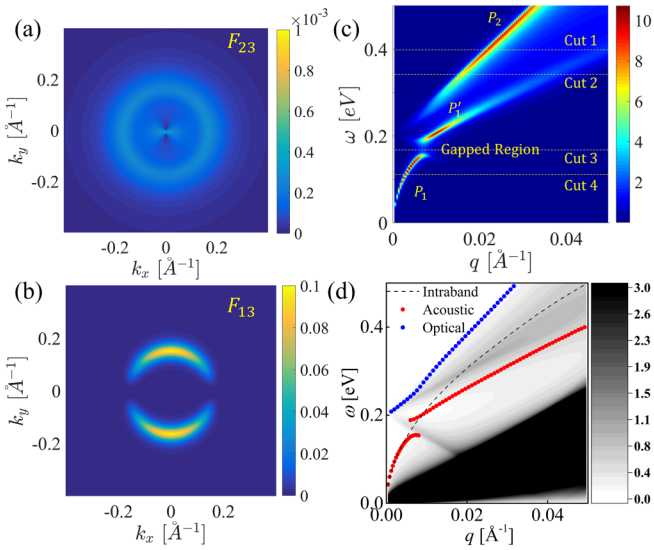

FIG. 3. (a) Calculated $S(\boldsymbol{q}, \omega)$ considering only the intraband transitions in Fig. 1(d), with the shaded region representing the formed intraband e-h continuums. κ is set to be 2 throughout this paper. (b) The interband overlapping integrals F_{23} and F_{13} at $q = 0.01$ Å^{-1}. (c) Calculated $S(\boldsymbol{q}, \omega)$ considering all the transition channels in Fig. 1(d). (d) Extracted peaks at each q in (c) (filled circles), together with the intraband plasmon mode (dashed line) and e-h continuums.

III. EMERGENT OPTICAL PLASMON MODE

Now we shift our focus to the detailed characterizations of the plasmon modes, especially the existence of the optical plasmon mode. Under the random phase approximation, the plasmon excitations can be obtained from the dielectric function $\varepsilon(q, \omega)$ as [30]

$$\varepsilon(\boldsymbol{q}, \omega) = 1 - V_q \Pi(\boldsymbol{q}, \omega), \tag{3}$$

where $V_q = 2\pi e^2/\kappa q$ is the 2D Coulomb interaction, κ is the effective dielectric constant. The noninteracting polarization function $\Pi(q, \omega)$ is expressed as [8]

$$\Pi(\boldsymbol{q}, \omega) = \sum_{l,l'} \int \frac{d^2\boldsymbol{k}}{(2\pi)^2} \frac{n(\xi_{l\boldsymbol{k}}) - n(\xi_{l'\boldsymbol{k}+\boldsymbol{q}})}{\omega + \xi_{l\boldsymbol{k}} - \xi_{l'\boldsymbol{k}+\boldsymbol{q}} + i\eta} F_{ll'(\boldsymbol{k},\boldsymbol{k}+\boldsymbol{q})}. \tag{4}$$

Here, $l(l')$ labels the band indexes, n is the Fermi distribution function, η is an infinitesimal introducing the damping, and $\xi_{l\boldsymbol{k}}$ represents the band dispersion. $F_{ll'}(\boldsymbol{k}, \boldsymbol{k}+\boldsymbol{q})$ has the form of

$$F_{ll'}(\boldsymbol{k}, \boldsymbol{k}+\boldsymbol{q}) = |\langle \boldsymbol{k}, l | l', \boldsymbol{k}+\boldsymbol{q} \rangle|^2, \tag{5}$$

where $|l, \boldsymbol{k}\rangle$ is the periodic part of the Bloch wave function. The plasmon excitations are defined by $\varepsilon(\boldsymbol{q}, \omega) = 0$ and usually manifested by the peaks in the energy-loss function as

$$S(\boldsymbol{q}, \omega) = \text{Im}\left[-\frac{1}{\varepsilon(\boldsymbol{q}, \omega)}\right], \tag{6}$$

which can be directly detected experimentally.

We first examine the plasmon excitations originating from the intraband transitions by setting $l = l'$ in Eq. (4). The results are shown in Fig. 3(a), displaying the three plasmon modes from the TSS, 2DEG, and their combined contributions, respectively, with each mode obeying the generic acoustic plasmon dispersion in 2D electron systems [31,32]. Here we note that, when compared to the commonly studied Dirac plasmon mode purely tied to the TSS, the resultant acoustic plasmon mode is energetically pushed higher in the presence of the 2DEG [33].

Now we turn to the interband transitions by first looking at the interband overlapping integrals $F_{l\neq l'}$ at a quantitative level. In ordinary systems, $F_{ll'}$ is negligibly small from the interband channels in the long-wavelength limit, as demanded by the orthogonality of the eigenstates. Here, in Fig. 3(b), we contrast F_{23} and F_{13} in the momentum space, displaying dramatically enhanced interband transitions in the latter within the gap opening region of the inverted bands [see Fig. 1(d)]. Another subtle point to emphasize is that the interband transitions are enhanced only between bands 1 and 3 with the same helicity.

Next we investigate the collective nature of the e-h pairs associated with the interband channels by letting the band indexes l and l' in Eq. (4) run over all the hybrid bands in Fig. 1(d). The calculated loss function $S(\boldsymbol{q}, \omega)$ is shown in Fig. 3(c), which exhibits two striking features. First, the acoustic plasmon mode is broken into two segments, labeled by P_1 and P_1'. To elucidate this effect more clearly, we plot in Fig. 3(d) all the locations of the peaked spectra extracted from

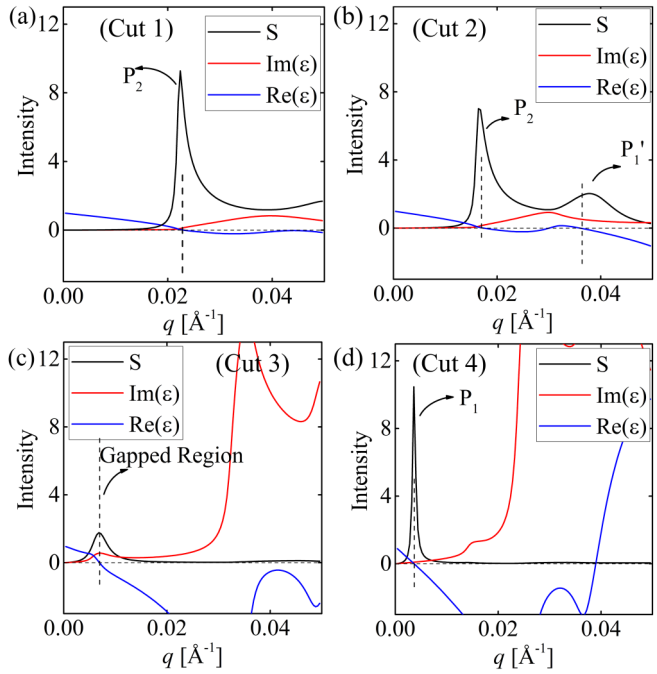

FIG. 4. Momentum distribution curves of the real (blue) and imaginary (red) parts of $\varepsilon(\boldsymbol{q}, \omega)$ and the loss function $S(\boldsymbol{q}, \omega)$ (black) along cuts 1–4 (dashed lines) indicated in Fig. 3(c).

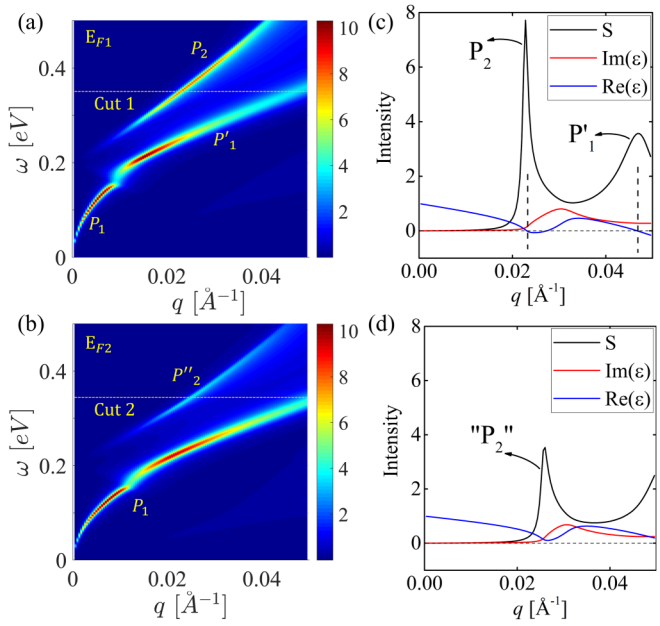

FIG. 5. (a), (b) The loss functions $S(\boldsymbol{q}, \omega)$ at the different doping levels marked as E_{F1} and E_{F2} in Fig. 1(d). (c), (d) Momentum distribution curves along cuts 1 and 2 in (a) and (b), respectively.

Fig. 3(c), revealing that the gap opening in the acoustic plasmon mode is primarily due to its coupling with the e-h pairs of the interband transitions. Second, and most significantly, an optical plasmon mode (P_2) emerges at higher frequencies, which originates from the enhanced interband transitions between the inverted bands 1 and 3 with the same helicity. The helicity selection rule of the optical plasmon excitation is in essence rooted in the fact that the originally trivial 2DEG has inherited the nontrivial topology from the TSS.

To further substantiate that the hybrid plasmon modes are well-defined and long living, we show in Fig. 4 the momentum dependence of the real and imaginary parts of the dielectric function $\varepsilon(\boldsymbol{q}, \omega)$ and the loss function $S(\boldsymbol{q}, \omega)$ along the four dashed lines marked in Fig. 3(c). We observe that the acoustic and optical plasmon modes both emerge at $\mathrm{Re}[\varepsilon(\boldsymbol{q}, \omega)] = 0$, with negligibly small $\mathrm{Im}[\varepsilon(\boldsymbol{q}, \omega)]$. Furthermore, the gap opening in the acoustic plasmon mode can be better understood by combining Figs. 3(d) and 4. Physically, the number of e-h pairs is proportional to the intensity of $\mathrm{Im}[\varepsilon(\boldsymbol{q}, \omega)]$ [26], which also determines the Landau damping rate of the plasmons. In Fig. 4(c), the $\mathrm{Im}[\varepsilon(\boldsymbol{q}, \omega)]$ shows a small peak near the lower boundary of the interband e-h continuum [see also in Fig. 3(d)]. As a consequence, the acoustic plasmon mode decays more quickly in this region, thereby opening a gap as shown in Figs. 3(c) and 3(d). It is worth noting that, given the magnitudes of the plasmon modes obtained in the present paper, the temperature effect is negligible on the plasmon dispersions as long as the temperature is not much higher than room temperature.

Now that the existence of this plasmon mode has been established, we can explore its other characteristics and in particular tunability in physically realistic conditions. First, we stress that its emergence with substantial spectral weight is ensured only when the band inversion takes place near the Fermi level. To illustrate this point, we can shift the Fermi level of the system to be away from the band inversion region by doping, indicated by the marked Fermi levels (E_{F1} and E_{F2}) in Fig. 1(d). The corresponding plasmon modes are shown in Figs. 5(a) and 5(b), revealing that the optical plasmon mode weakens in Fig. 5(a) and disappears in Fig. 5(b). In particular, peak P_2 is contributed by uncorrelated e-h pairs rather than a true plasmon mode, as reflected in Fig. 5(d) by nonzero $\mathrm{Re}[\varepsilon(\boldsymbol{q}, \omega)]$ and strong damping in $\mathrm{Im}[\varepsilon(\boldsymbol{q}, \omega)]$. Second, there exists a subtle conservation law in the total spectral weight of the plasmon modes, as shown in Fig. S(6) by the integrated $S(\boldsymbol{q}, \omega)$ over ω at each q from Figs. 3(c) and S4(c), respectively. The underlying physics is that, generically, electrons in the occupied states can only participate in either the intra- or inter-band transitions even in the hybridized case, but not both.

IV. DISCUSSION AND CONCLUSION

Before closing, we propose two opposite tuning approaches to further explore the characteristics of the optical plasmon mode. One is to completely deplete the 2DEG through surface hole doping [4], which should be accompanied by the disappearance of the optical plasmon mode. The other is to increase the density of 2DEG, so more than one spin-degenerate states will drop below the CBM and be coupled with the TSS. As illustrated in Fig. S5 of the SM, both sets of the spin-degenerate states can contribute to the optical plasmon mode within the helicity selection rule, with higher frequency and overall enhanced spectral weight [see Fig. S(6)]. This latter regime is more experimentally reachable, as indicated in several recent studies [18–22].

In conclusion, we have presented a comprehensive theoretical study of the coupling between the TSS and 2DEG at the surface of topological insulators, with multiple intriguing findings. We first revealed that the helicity of the former can be effectively shared with the latter through proximity effect. Next we predicted that the combined system can harbor an optical plasmon mode, which is solely attributed to the interband transitions between the two types of surface states with the same helicity, and the dominant contribution is drawn from the band inverted region. The allowance of the interband transitions necessarily also introduces pronounced variations in the Dirac plasmon mode, characterized by a gapped feature. The existence and tunability of this optical plasmon mode can be experimentally exploited for applications in plasmonic and spintronic devices based on topological insulators.

ACKNOWLEDGMENTS

We thank Dr. Q. Niu for helpful discussions. This work is supported by the National Key R&D Program of China (Grant No. 2017YFA0303500), the National Natural Science Foundation of China (Grants No. 11634011, No. 11974323, No. 11874268, and No. 12004368), the Anhui Initiative in Quantum Information Technologies (Grant No. AHY170000), the Strategic Priority Research Program of Chinese Academy of Sciences (Grant No. XDB30000000), and the China Postdoctoral Science Foundation (Grant No. 2020M671859).

[1] D. Hsieh, D. Qian, L. Wray, Y. Xia, Y. S. Hor, R. J. Cava, and M. Z. Hasan, A topological Dirac insulator in a quantum spin Hall phase, Nature (London) **452**, 970 (2008).

[2] H. Zhang, C. X. Liu, X. L. Qi, X. Dai, Z. Fang, and S. C. Zhang, Topological insulators in Bi_2Se_3, Bi_2Te_3 and Sb_2Te_3 with a single Dirac cone on the surface, Nat. Phys. **5**, 438 (2009).

[3] Y. L. Chen, J. G. Analytis, J. H. Chu, Z. K. Liu, S. K. Mo, X. L. Qi, H. J. Zhang, D. H. Lu, X. DAi, Z. Fanf, S. C. Zhang, I. R. Fisher, Z. Hussain, and Z. X. Shen, Experimental realization of a three-dimensional topological insulator, Bi_2Te_3, Science **325**, 178 (2009).

[4] D. Hsieh, Y. Xia, D. Qian, L. Wray, J. H. Dil, F. Meier, J. Osterwalder, L. Patthey, J. G. Checkelsky, N. P. Ong, A. V. Fedorov, H. Lin, A. Bansil, D. Grauer, Y. S. Hor, R. J. Cava, and M. Z. Hasan, A tunable topological insulator in the spin helical Dirac transport regime, Nature (London) **460**, 1101 (2009).

[5] D. Hsieh, Y. Xia, D. Qian, L. Wray, F. Meier, J. H. Dil, J. Osterwalder, L. Patthey, A. V. Fedorov, H. Lin, A. Bansil, D. Grauer, Y. S. Hor, R. J. Cava, and M. Z. Hasan, Observation of Time-Reversal-Protected Single-Dirac-Cone Topological-Insulator States in Bi_2Te_3 and Sb_2Te_3, Phys. Rev. Lett. **103**, 146401 (2009).

[6] Y. Zhang, K. He, C. Z. Chang, C. L. Song, L.-L. Wang, X. Chen, J. F. Jia, Z. Fang, X. Dai, W. Y. Shan, S. Q. Shen, Q. Niu, X. L. Qi, S. C. Zhang, X. C. Ma, and Q. K. Xue, Crossover of the three-dimensional topological insulator Bi_2Se_3 to the two-dimensional limit, Nat. Phys. **6**, 584 (2010).

[7] S. Raghu, S. B. Chung, X. L. Qi, and S. C. Zhang, Collective Modes of a Helical Liquid, Phys. Rev. Lett. **104**, 116401 (2010).

[8] F. Zhang, J. Zhou, D. Xiao, and Y. Yao, Tunable Intrinsic Plasmons Due to Band Inversion in Topological Materials, Phys. Rev. Lett. **119**, 266804 (2017).

[9] P. Di Pietro, M. Ortolani, O. Limaj, A. Di Gaspare, V. Giliberti, F. Giorgianni, M. Brahlek, N. Bansal, N. Koirala, S. Oh, P. Calvani, and S. Lupi, Observation of Dirac plasmons in a topological insulator, Nat. Nanotechnol. **8**, 556 (2013).

[10] A. Politano, V. M. Silkin, I. A. Nechaev, M. S. Vitiello, L. Viti, Z. S. Aliev, M. B. Babanly, G. Chiarello, P. M. Echenique, and E. V. Chulkov, Interplay of Surface and Dirac Plasmons in Topological Insulators: The Case of Bi_2Se_3, Phys. Rev. Lett. **115**, 216802 (2015).

[11] Y. D. Glinka, S. Babakiray, T. A. Johnson, M. B. Holcomb, and D. Lederman, Nonlinear optical observation of coherent acoustic Dirac plasmons in thin-film topological insulators, Nat. Commun. **7**, 13054 (2016).

[12] X. Jia, S. Zhang, R. Sankar, F. C. Chou, W. Wang, K. Kempa, E. W. Plummer, J. Zhang, X. Zhu, and J. Guo, Anomalous Acoustic Plasmon Mode from Topologically Protected States, Phys. Rev. Lett. **119**, 136805 (2017).

[13] S. Xue, M. Wang, Y. Li, S. Zhang, X. Jia, J. Zhou, Y. Shi, X. Zhu, Y. Yao, and J. Guo, Observation of Nodal-Line Plasmons in ZrSiS, Phys. Rev. Lett. **127**, 186802 (2021).

[14] M. Bianchi, D. Guan, S. Bao, J. Mi, B. B. Iversen, P. D. King, and P. Hofmann, Coexistence of the topological state and a two-dimensional electron gas on the surface of Bi_2Se_3, Nat. Commun. **1**, 128 (2010).

[15] T. Ando, A. B. Fowler, and F. Stern, Electronic properties of two-dimensional systems, Rev. Mod. Phys. **54**, 437 (1982).

[16] S. Abe, T. Inaoka, and M. Hasegawa, Evolution of electron states at a narrow-gap semiconductor surface in an accumulation-layer formation process, Phys. Rev. B **66**, 205309 (2002).

[17] P. D. C. King, T. D. Veal, and C. F. McConville, Nonparabolic coupled Poisson-Schrödinger solutions for quantized electron accumulation layers: Band bending, charge profile, and subbands at InN surfaces, Phys. Rev. B **77**, 125305 (2008).

[18] L. A. Wray, S.-Y. Xu, Y. Xia, D. Hsieh, A. V. Fedorov, Y. S. Hor, R. J. Cava, A. Bansil, H. Lin, and M. Z. Hasan, A topological insulator surface under strong Coulomb, magnetic and disorder perturbations, Nat. Phys. **7**, 32 (2011).

[19] H. M. Benia, C. Lin, K. Kern, and C. R. Ast, Reactive Chemical Doping of the Bi_2Se_3 Topological Insulator, Phys. Rev. Lett. **107**, 177602 (2011).

[20] M. Bianchi, R. C. Hatch, J. Mi, B. B. Iversen, and P. Hofmann, Simultaneous Quantization of Bulk Conduction and Valence States Through Adsorption of Nonmagnetic Impurities on Bi_2Se_3, Phys. Rev. Lett. **107**, 086802 (2011).

[21] P. D. King, R. C. Hatch, M. Bianchi, R. Ovsyannikov, C. Lupulescu, G. Landolt, B. Slomski, J. H. Dil, D. Guan, J. L. Mi, E. D. Rienks, J. Fink, A. Lindblad, S. Svensson, S. Bao,

G. Balakrishnan, B. B. Iversen, J. Osterwalder, W. Eberhardt, F. Baumberger *et al.*, Large Tunable Rashba Spin Splitting of a Two-Dimensional Electron Gas in Bi_2Se_3, Phys. Rev. Lett. **107**, 096802 (2011).

[22] Z. H. Zhu, G. Levy, B. Ludbrook, C. N. Veenstra, J. A. Rosen, R. Comin, D. Wong, P. Dosanjh, A. Ubaldini, P. Syers, N. P. Butch, J. Paglione, I. S. Elfimov and A. Damascelli, Rashba Spin-Splitting Control at the Surface of the Topological Insulator Bi_2Se_3, Phys. Rev. Lett. **107**, 186405 (2011).

[23] W. Y. Shan, H. Z. Lu, and S. Q. Shen, Effective continuous model for surface states and thin films of three-dimensional topological insulators, New J. Phys. **12**, 043048 (2010).

[24] J. Zhang, C. Triola, and E. Rossi, Proximity Effect in Graphene-Topological-Insulator Heterostructures, Phys. Rev. Lett. **112**, 096802 (2014).

[25] See Supplemental Material at http://link.aps.org/supplemental/10.1103/PhysRevB.105.205408 for more detailed derivations and supplemental figures.

[26] X. Li, D. Xiao, and Z. Zhang, Landau damping of quantum plasmons in metal nanostructures, New J. Phys. **15**, 023011 (2013).

[27] G. Khalsa, B. Lee, and A. H. MacDonald, Theory of t_{2g} electron-gas Rashba interactions, Phys. Rev. B **88**, 041302(R) (2013).

[28] J. H. Zhou, W. Y. Shan, and D. Xiao, Spin responses and effective Hamiltonian for the two-dimensional electron gas at the oxide interface $LaAlO_3/SrTiO_3$, Phys. Rev. B **91**, 241302(R) (2015).

[29] L. Fu, HexagonalWarping Effects in the Surface States of the Topological Insulator Bi_2Te_3, Phys. Rev. Lett. **103**, 266801 (2009).

[30] D. Pines, *Elementary Excitations in Solids: Lectures on Protons, Electrons, and Plasmons* (Westview Press, Boulder, 1999), Vol. 5.

[31] R. E. V. Profumo, R. Asgari, M. Polini, and A. H. MacDonald, Double-layer graphene and topological insulator thin-film plasmons, Phys. Rev. B **85**, 085443 (2012).

[32] E. H. Hwang and S. Das Sarma, Dielectric function, screening, and plasmons in two-dimensional graphene, Phys. Rev. B **75**, 205418 (2007).

[33] T. Stauber, G. Gómez-Santos, and L. Brey, Spin-charge separation of plasmonic excitations in thin topological insulators, Phys. Rev. B **88**, 205427 (2013).